

Electronic structure of sodium tungsten bronzes Na_xWO_3 by high-resolution angle-resolved photoemission spectroscopy

S. Raj,^{1,*} H. Matsui,¹ S. Souma,^{1,2} T. Sato,^{1,2} T. Takahashi,^{1,2} A. Chakraborty,³ D. D. Sarma,^{3,4,†} P. Mahadevan,⁵ S. Oishi,⁶ W. H. McCarrroll,⁷ and M. Greenblatt⁸

¹Department of Physics, Tohoku University, Sendai 980-8578, Japan

²CREST, Japan Science and Technology Agency (JST), Kawaguchi 332-0012, Japan

³Solid State and Structural Chemistry Unit, Indian Institute of Science, Bangalore 560 012, India

⁴Centre for Advanced Materials, Indian Association for the Cultivation of Science, Kolkata 700 032, India

⁵S. N. Bose National Centre for Basic Sciences, JD Block, Sector 3, Salt Lake, Kolkata 700 098, India

⁶Faculty of Engineering, Shinshu University, Nagano 380-8553, Japan

⁷Department of Chemistry and Biochemistry, Rider University, New Jersey 08648, USA

⁸Department of Chemistry and Chemical Biology, The State University of New Jersey, New Jersey 08854, USA

(Received 12 July 2006; revised manuscript received 13 November 2006; published 25 April 2007)

The electronic structure of sodium tungsten bronzes, Na_xWO_3 , for full range of x is investigated by high-resolution angle-resolved photoemission spectroscopy (HR-ARPES). The experimentally determined valence-band structure has been compared with the results of *ab initio* band-structure calculation. The HR-ARPES spectra taken in both the insulating and metallic phase of Na_xWO_3 reveal the origin of metal-insulator transition (MIT) in the sodium tungsten bronze system. In the insulating Na_xWO_3 , the near- E_F states are localized due to the strong disorder caused by the random distribution of Na^+ ions in WO_3 lattice. While the presence of an impurity band (level) induced by Na doping is often invoked to explain the insulating state found at low concentrations, there is no signature of impurity band (level) found from our results. Due to disorder and Anderson localization effect, there is a long-range Coulomb interaction of conduction electrons; as a result, the system is insulating. In the metallic regime, the states near E_F are populated and the Fermi level shifts upward rigidly with increasing electron doping (x). The volume of electronlike Fermi surface (FS) at the $\Gamma(X)$ point gradually increases with increasing Na concentration due to W $5d_{2g}$ band filling. A rigid shift of E_F is found to give a qualitatively good description of the FS evolution.

DOI: 10.1103/PhysRevB.75.155116

PACS number(s): 79.60.-i, 71.30.+h, 71.18.+y

I. INTRODUCTION

Tungsten oxide based materials have created tremendous interest among material physicists because of their potential technological implications. Bulk WO_3 modified by ion incorporation (A_xWO_3) or substoichiometry (WO_3) exhibits many technologically important properties.^{1,2} It is possible to insert sodium (Na) in bulk WO_3 , thus forming the series of sodium tungsten bronzes. Na_xWO_3 shows very interesting optical properties³ and the color changes from yellowish green to gray, blue, deep violet, red, and finally to gold as x increases from zero to unity, as shown in Fig. 1(a). The electronic, optical, and transport properties of sodium tungsten bronzes have been studied extensively. The metal-insulator transition (MIT) observed as a function of x is one of the most interesting electronic properties in Na_xWO_3 . A high metallic conduction is obtained for $x \geq 0.25$, and the system undergoes MIT with decreasing x .⁴ Hence, the study of the electronic structure of Na_xWO_3 is of great interest from both technological and fundamental perspectives.

Na_xWO_3 shows a very rich phase diagram⁵ with increasing x , as shown in Fig. 1(b), which is also interesting to study from the structural evolution point of view. The crystal structure changes from monoclinic, to orthorhombic, to tetragonal, and finally to cubic with increasing x . For $x \leq 0.4$, it exists in a variety of structural modifications, while for $x \geq 0.5$, Na_xWO_3 is highly metallic with perovskite-type crystal structure with cubic crystal symmetry. For highly metallic

Na_xWO_3 , Brown and Banks⁶ have shown that the crystal lattice parameter increases linearly with x [$a = 3.7845 + 0.0820x$ (Å)]. Figure 1(c) shows the crystal structure of NaWO_3 . Na ions occupy the center of the cube, while the WO_6 octahedra are located at the cube corners. The octahedral crystal field of the six oxygen neighbors of the W split the W $5d$ bands into triply degenerate t_{2g} and doubly degenerate e_g bands (in the cubic phase, when the WO_6 octahedra are distorted, the degeneracy of these levels may be lifted further due to lowering of the symmetry). In WO_3 , the Fermi level (E_F) lies at the top of the O $2p$ bands, and WO_3 is a band insulator. Within a rigid-band model, as shown schematically in Fig. 1(d), the band structure of both WO_3 and NaWO_3 should be identical, with E_F at different positions. In Na_xWO_3 , the Na $3s$ electrons are transferred into the W $5d_{2g}$, π^* band and the system should behave metallic for any value of x . However, for low concentration of $x \leq 0.25$, the material is insulating and the origin of the MIT is still under debate. There are three theoretical models to explain the observed MIT in Na_xWO_3 . According to the Anderson localization model,⁷ the random distribution of Na^+ ions in the WO_3 lattice gives rise to strong disorder effects, which leads to the localization of states at the conduction-band tail and the system undergoes an MIT for low Na concentration. An alternative explanation for the MIT is the development of an impurity band (level)⁸ induced by Na doping, where the states become localized at low Na concentration. Another possibility of driving the MIT is the splitting of the band due

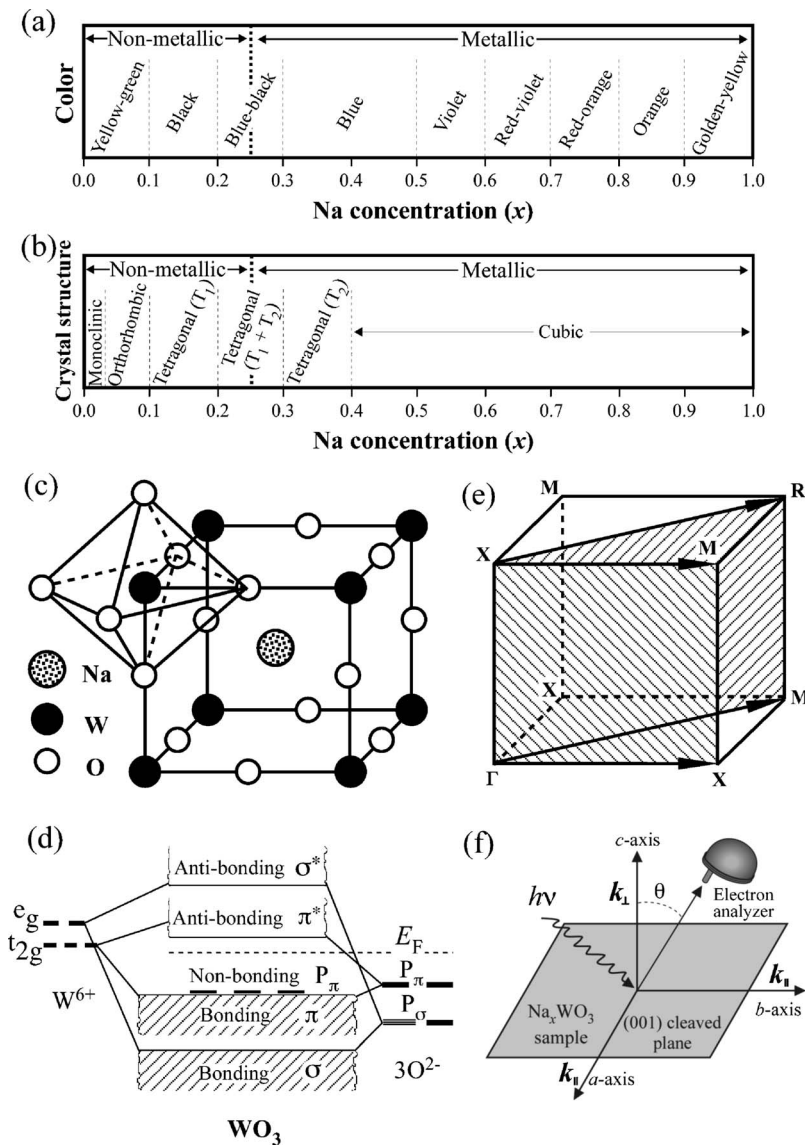


FIG. 1. Schematic view of (a) optical properties and (b) phase diagram of the Na_xWO_3 system with Na concentration (x). (c) Cubic crystal structure of NaWO_3 . (d) Rigid-band model for WO_3 showing the Fermi level E_F in between the bottom of conduction band and the top of valence band. (e) Cubic Brillouin zone showing highly symmetric lines of NaWO_3 . (f) Geometrical arrangement for the ARPES measurements.

to electron correlation at the chemical potential (or E_F),⁹ where the localization occurs in a pseudogap between the separated bands. Among the various models proposed to explain the MIT in Na_xWO_3 , there is, however, evidence in favor of each of these possibilities. Hence, no conclusion has been made as yet, and it needs to be investigated more deeply and thoroughly.

The localization and delocalization of states associated with MIT occurs in a very narrow range of energy close to E_F in Na_xWO_3 ; hence, photoemission spectroscopy is one of the appropriate tools to elucidate the mechanism of MIT. Most of the published angle-integrated photoemission literatures^{10–13} were not able to resolve the mechanism of MIT. Höchst *et al.*¹⁴ have performed angle-resolved photoemission spectroscopy (ARPES) on metallic $\text{Na}_{0.85}\text{WO}_3$ single crystal with relatively low energy and momentum resolution, and to our knowledge no further systematic ARPES results are available for a full range of x . Moreover, due to the previous low energy and angular resolution of the experimental data, it is difficult to compare the experimental results with available band calculations.^{15–17} The evolution

of electronic structure with x in the metallic regime is also not clear from the previous studies. Hence, high-resolution ARPES (HR-ARPES) is absolutely necessary to experimentally establish the band structure, evolution of electronic structure with Na doping, and to elucidate the mechanism of MIT in Na_xWO_3 .

In this paper, we report HR-ARPES on both insulating ($x=0.025$) and metallic ($x=0.3, 0.58, 0.65, 0.7, \text{ and } 0.8$) Na_xWO_3 . The valence-band structure and the Fermi surface (FS) have been established experimentally. We have also carried out *ab initio* band-structure calculations based on the plane-wave pseudopotential method and compared it with experimental results.

For the insulating sample, the variation of the density of states near E_F suggests an Anderson-type localization of carriers for the ground state in lightly doped Na_xWO_3 . The formation of polaron in low-doped tungsten bronze is also discussed from the temperature variation of photoemission spectra. In highly metallic Na_xWO_3 , the FS shows an electronlike pocket centered at the $\Gamma(X)$ point in the Brillouin zone (BZ) [Fig. 1(e)], in good agreement with the band cal-

ulation. The volume of FS monotonically increases with x , indicating that Na $3s$ electrons go into the $W 5dt_{2g}$, π^* conduction band and the states near E_F are filled with Na doping. A simple rigid-band shift can well explain the x -dependent band structure in highly metallic Na_xWO_3 , where the doped electrons merely fill up the conduction band.

II. EXPERIMENTS

Single crystals of insulating Na_xWO_3 ($x=0.025$) were grown from high-temperature solution of Na_2O-WO_3 by a slow cooling method.¹⁸ The crystals were found to have orthorhombic structure with lattice parameters $a = 7.311 \pm 0.003$ Å, $b = 7.523 \pm 0.003$ Å, and $c = 3.85 \pm 0.001$ Å. Metallic single crystals of Na_xWO_3 ($x=0.3, 0.58, 0.65, 0.7$, and 0.8) were grown by the fused salt electrolysis of Na_2WO_4 and WO_3 as described by Shanks.¹⁹ The resistivity measurements show that the crystals are metallic and the x values were obtained from the measured lattice parameters, as described by Brown and Banks.⁶

HR-ARPES measurements were performed with a Gammadata-Scienta SES 200 spectrometer with a high-flux discharge lamp and a toroidal grating monochromator. The He 1α ($h\nu=21.218$ eV) resonance line was used to excite photoelectrons. The geometrical arrangement for the ARPES measurements is shown in Fig. 1(f). The incoming photons and outgoing electrons lie in a plane normal to the crystal surface. The crystal surface is rotated 24° to cover the full first BZ ($\Gamma \rightarrow X$) at He 1α photon energy. The energy and angular (momentum) resolutions were set at 5–11 meV and 0.2° (0.01 Å $^{-1}$), respectively. The measurements were performed at 50–300 K for insulating and 14 K for metallic Na_xWO_3 in a vacuum better than 3×10^{-11} Torr base pressure. A clean surface of the sample for photoemission measurements was obtained by *in situ* cleaving along the (001) surface. HR-ARPES spectra were measured for the two high-symmetry directions, namely, $\Gamma(X)-X(M)$ and $\Gamma(X)-M(R)$, as shown in Fig. 1(e). All the spectra were collected within 24 h after cleaving, during which we did not observe any significant changes in the spectra indicative of the contamination and/or degradation of the sample surface. The Fermi level (E_F) of the sample was referred to that of a gold film evaporated on the sample substrate.

III. BAND CALCULATIONS

We have performed *ab initio* band-structure calculations for WO_3 and $NaWO_3$ using projected augmented wave potential^{20,21} as implemented in the Vienna *ab initio* simulation package (VASP) code.²² A k -point mesh of $8 \times 8 \times 8$ with lattice constants of 3.78 and 3.86 Å for WO_3 and $NaWO_3$, respectively, and the generalized gradient approximation (GGA) for the exchange were used for the calculation. We have simulated electron doping in our calculations by a rigid-band shift of the band structure and the corresponding calculated Fermi surfaces have been compared with experiment. Since the GGA exchange based calculations have the drawback of underestimating the band gap, we use the scissor

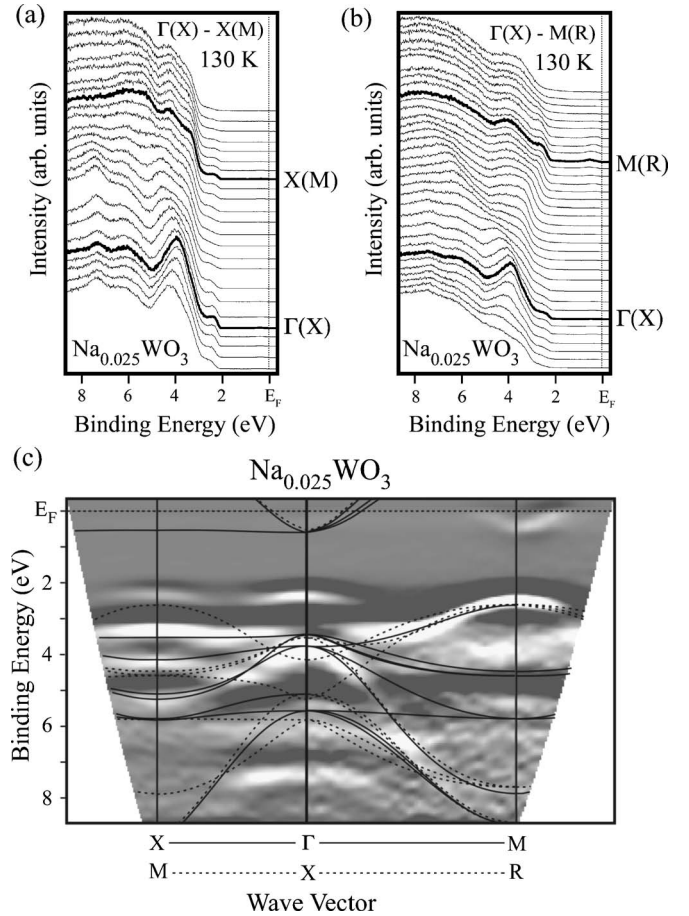


FIG. 2. Valence-band HR-ARPES spectra of Na_xWO_3 for $x=0.025$ measured along (a) $\Gamma(X)-X(M)$ and (b) $\Gamma(X)-M(R)$ directions at 130 K. (c) Experimental valence-band structure obtained from HR-ARPES experiments at 130 K. Bright areas correspond to the experimental bands. The theoretical band calculation of WO_3 after shifting E_F is also shown by thin solid and dashed lines for comparison.

operator technique to independently align the calculated valence- and conduction-band structures with experiment.

IV. RESULTS AND DISCUSSION

A. Valence-band region

1. Insulating regime

We have measured valence-band HR-ARPES spectra of insulating Na_xWO_3 for $x=0.025$, which has x well below the critical composition, at 130 K. Figures 2(a) and 2(b) show HR-ARPES spectra along $\Gamma(X)-X(M)$ and $\Gamma(X)-M(R)$ directions in the BZ, respectively. In Na_xWO_3 , E_F is situated in the conduction band for all the compositions. The bottom of the conduction band in Na_xWO_3 for $x=0.025$ lies at 0.5 eV binding energy [clearly visible around the $M(R)$ point], whereas the top of the valence band extends up to 2.5 eV, indicating a large (~ 2 eV) energy gap. This large gap corresponds to the hard band gap observed in insulating WO_3 . The most prominent peak observed in the valence band is at

4.0 eV (in both highly symmetric directions) along with two other broad peaks at 6.0 and 7.4 eV around the $\Gamma(X)$ point, which disperse downward while moving toward the zone boundaries. In Fig. 2(c), we show the experimental valence-band structure of Na_xWO_3 for $x=0.025$ and it has been obtained by taking the second derivative of the HR-ARPES spectra shown in Figs. 2(a) and 2(b). The pseudopotential band structure for cubic WO_3 is also presented for comparison. We shift the calculated E_F of WO_3 upward to overlap with the experimental bands. We find dispersive bands at $X(M)$ and $M(R)$ points which are not predicted in the band calculation. The top of the valence band at 2.5 eV and the band at 7.4 eV around $\Gamma(X)$ point are also not predicted in the band calculation. Nevertheless, the band around 4.0 eV at $\Gamma(X)$, which highly disperses along both $\Gamma(X)$ - $X(M)$ and $\Gamma(X)$ - $M(R)$ directions, is in good agreement with the band calculation. It is found from the band calculation that the valence band of Na_xWO_3 for $x=0.025$ consists of mostly the O $2p$ states along with a small admixture of bonding W $5d_{eg}$ states.

Now, we discuss the discrepancy between the pseudopotential band calculation and experimentally determined band structure. Although many bands are in good agreement with the band calculation but few bands along with its dispersion are not predicted in the theoretical band calculation. There could be various reasons for the observed mismatch. The first reason is the neglect of final-state effects in our approach. Depending on the initial photon energy that is used, the final state of the electron could be into the unoccupied states which are not necessarily free-electron-like as discussed in the literature.^{23,24} For low photon energies, one could have the problem of there being no states satisfying the requisite selection rules for the final-state electron to make the transition into. This results in strong attenuation of the intensity in the experimental spectra at specific k points. More details may be found in Ref. 25. Another source of deviation due to final-state effects arises from the electron mean free path. As this is limited by inelastic electron scattering due to the electron-electron and electron-phonon interactions, one has a k broadening into the final state. In fact, this can give rise to an intrinsic shift of the photoemission peaks.²⁶ The second source of deviation could arise from the fact that the approach we use treats correlations in a mean-field way, while in reality this might not be the case and many-body effects might be needed to explain the picture. Finally, there could be the effects resulting from the presence of defects which could modify the band structure from that of the perfect crystal considered in the present study. However, one can use different photon energies or use complementary probes such as very low-energy electron diffraction or inverse photoemission spectroscopy to distil out the artifacts due to final-state effects in experiment.^{27,28}

To investigate the temperature dependence of the valence-band spectra, we carried out photoemission spectroscopy (PES) of Na_xWO_3 for $x=0.025$ around the $\Gamma(X)$ point (within acceptance angle of detector) with variation of temperature, and the results are shown in Fig. 3(a). Our PES spectra see mostly the angle integrated around the $\Gamma(X)$ point, and all the spectra are normalized under the curve within the energy

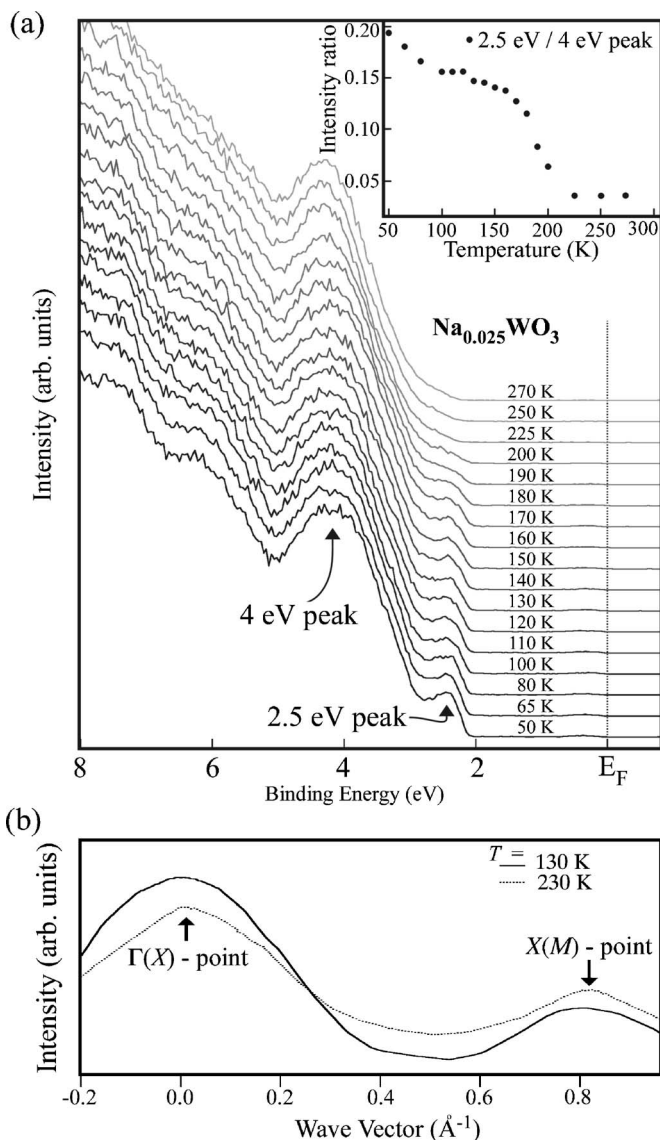


FIG. 3. (a) Valence-band PES spectra of Na_xWO_3 for $x=0.025$ at several temperatures showing the signature of polaron formation at the valence-band edge, 2.5 eV. The inset shows the temperature dependence of the intensity ratio of the 2.5 eV peak to the 4.0 eV peak. (b) Intensity variation of 2.5 eV peak with respect to wave vector k along the $\Gamma(X)$ - $X(M)$ direction at 130 and 230 K.

range shown in the figure. We clearly observe the variation of the intensity of the 2.5 eV peak with temperature. The existence of 2.5 eV peak at the $\Gamma(X)$ point is not predicted from the band calculation. The band calculation is for cubic WO_3 , whereas the real sample is not a perfect cubic crystal structure with distorted octahedra.

We found that the 2.5 eV binding-energy feature at the $\Gamma(X)$ point and few other bands in valence-band region do not have good correspondence to the theoretical band calculation. To investigate whether these bands are arising due to surface states and/or surface resonance and/or umklapp bands, we have carried out PES with He II ($h\nu=40.8$ eV) photons, which is much more surface sensitive than He I photons. A surface state or surface resonance is localized at the surface and will not disperse in k_{\perp} . The two-dimensional

character of these states can be verified by probing their k_{\perp} dependence by changing photon energy. Generally, surface states are recognized as faint emissions but are not sufficient to identify unambiguously, because other structures such as umklapp bands may also appear in the data and confuse the observation of faint emissions. Umklapp transitions are related to bulk transitions via a reciprocal vector translation; they are well recognized in normal emissions. These emissions are directly related to the periodic structure of the sample and express with the reciprocal vector of the lattice. If the crystal has no surface reconstruction, then the umklapp processes have identical effects as bulk bands. Though the insulating system shows surface reconstruction (discussed later), we do not observe much difference in valence-band structure between insulating and metallic systems. From our experiment with He II photons, we did not see any reasonable density of states (DOS) at 2.5 eV, suggesting a three-dimensional description of this band implying its bulk origin. These experimental results suggest that the 2.5 eV feature does not arise from a surface state.

It is believed that at low sodium doping levels, the sodium tungsten bronzes are nonmetallic with localized W^{5+} and W^{6+} ions and show polaronic states.^{29,30} Polaron can form in the insulating system, particularly when the conduction electrons are in a comparatively narrow d band and are contributed by donors distributed at random in the lattice. The polaron formation in the lightly doped tungsten bronzes was studied with electron-spin resonance, optical absorption, and Raman spectroscopy.^{29,31} The conduction electrons are self-trapped by inducing an asymmetric local deformation of the lattice. Even if the electron is confined to a single lattice site, this type of trapping does not imply localization. The tunneling between different lattice sites is still relevant and a self-trapped carrier resides in an itinerant polaron state.³² This is most likely to occur when the band edge is degenerate and the valence-band edge is more often degenerate than the conduction-band edge, so that holes are more likely to be self-trapped than electrons. In the inset of Fig. 3(a), we show the intensity ratio of valence-band edge (2.5 eV peak) to 4 eV peak. We find that the intensity of 2.5 eV peak decreases with increasing temperature and reaches a minimum above 225 K. We think that the decrease in the intensity of 2.5 eV peak is due to the breakdown of polaron formation at higher temperatures (above 225 K). Above this temperature, the holes and/or electrons are no longer self-trapped. To study how this 2.5 eV peak behaves with respect to wave vector k at different temperatures, we measured the HR-ARPES spectra at 230 K (not shown) and clearly observe the decrease in intensity of the 2.5 eV peak around $\Gamma(X)$ as compared to 130 K. We have plotted the intensity variation of the 2.5 eV peak with respect to k along the $\Gamma(X)$ - $X(M)$ direction for 130 and 230 K, and the result is shown in Fig. 3(b). We observe the decrease in intensity around the $\Gamma(X)$ point as we move from 130 to 230 K, whereas the intensity increases at other k points away from the $\Gamma(X)$ point ($k=0$). Polaron can be considered as a local deformation and/or defect in the lattice and a truly localized defect level is derived primarily from the Γ point ($k=0$) with far less weight from other k points. A more delocalized defect level is derived from k

points other than Γ .³³ To our knowledge, the temperature dependence of the polaronic features is the first observation of the dynamics of the polaron in Na_xWO_3 . As the polaron becomes more delocalized, there is spectral weight transfer from Γ point to other k points. In Fig. 3(a), we mainly observe the intensity around the Γ point, and as a result, the intensity decreases with increasing temperature. The optical absorption of W^{5+} in WO_3 also shows the signature of polaron formation at low temperature and vanishes at 300 K.²⁹ This adds additional support to our conclusion that the increase in intensity of the valence-band edge below 225 K is likely due to the formation of polaron. The polaron can split and/or broaden the edge of the valence band, but due to the temperature-induced broadening in the spectra, we did not find any significant splitting and/or broadening of the band edge with temperature. This 2.5 eV feature survives into the metallic regime. The weakly dispersive nature of the states suggests that the presence of intrinsic defects could be a possible origin. Earlier work on perovskite oxides³⁴ has shown that oxygen vacancy states are induced at the top of the valence band, and these states by nature of their origin are weakly dispersive. Hence, we interpret the 2.5 eV feature as arising from the polaronic state formed by oxygen vacancies, which exhibits strong temperature dependence at low concentrations. This feature survives into the metallic regime, which suggests that there must be an alternate explanation to that provided earlier.

2. Metallic regime

The valence-band HR-ARPES spectra of metallic Na_xWO_3 for $x=0.3, 0.58, 0.65, 0.7,$ and 0.8 are measured at 14 K with He 1α photons along the high-symmetry lines in the BZ. Typical HR-ARPES spectra of Na_xWO_3 for $x=0.8$ are shown in Figs. 4(a) and 4(b) along the $\Gamma(X)$ - $X(M)$ and $\Gamma(X)$ - $M(R)$ directions, respectively. We can see a large (~ 2 eV) energy gap between the bottom of the conduction band and the top of the valence band similar to Na_xWO_3 for $x=0.025$ (see Fig. 2). A clear Fermi edge is visible in these metallic compounds. There are three prominent peaks (marked as $A, B,$ and C) visible around the $\Gamma(X)$ point. In Na_xWO_3 for $x=0.3$, the peaks are not very sharp due to the presence of disorder. A nondispersive peak at the top of the valence band at the $\Gamma(X)$ point gradually loses its intensity while moving toward zone boundaries and once again becomes prominent at zone boundaries. For $x=0.58, 0.65, 0.7,$ and 0.8 , the most prominent peak in the valence band is seen around 4.1–4.3 eV at the $\Gamma(X)$ point and disperses downward around the $\Gamma(X)$ point. All the spectral features are essentially similar in all compounds. However, in the $\Gamma(X)$ - $X(M)$ direction, the intense peak at 4.3 eV does not disperse as compared to the $\Gamma(X)$ - $M(R)$ direction [see Figs. 4(a) and 4(b)]. Two peaks [marked as B_1 and B_2 in Fig. 4(b)] between 4 and 6 eV merge to a single intense peak around 4.3 eV at $\Gamma(X)$. With increasing Na concentration in highly metallic Na_xWO_3 , all the peaks become more intense and sharper. This is attributed to the decrease of disorder in the system. No additional bands are found to emerge in the relevant energy window with Na doping, which suggest that a rigid-band model is adequate.

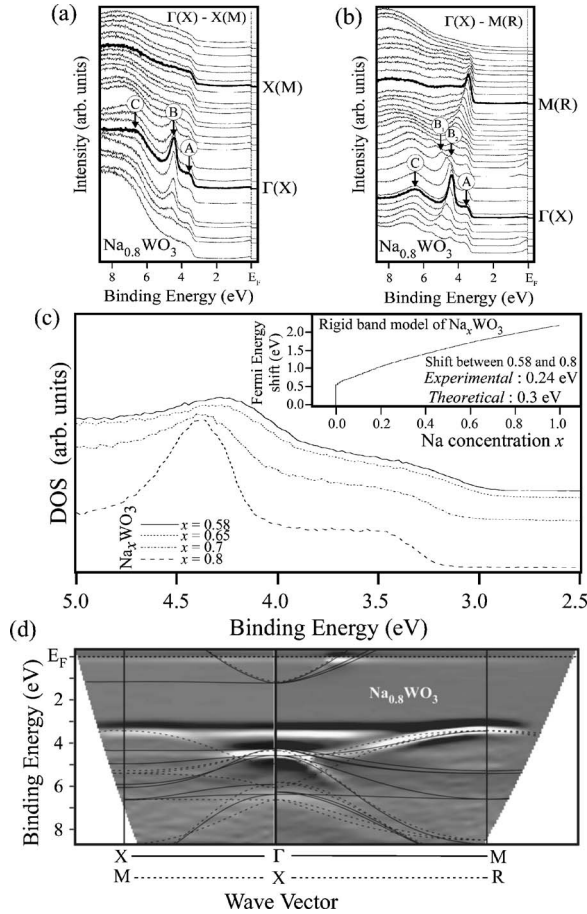


FIG. 4. Typical valence-band HR-ARPES spectra of Na_xWO_3 for $x=0.8$ measured at 14 K with He I α photons (21.218 eV) along (a) $\Gamma(X)$ - $X(M)$ and (b) $\Gamma(X)$ - $M(R)$ directions. (c) Comparison of HR-ARPES spectra near valence-band edge in highly metallic Na_xWO_3 for $x=0.58, 0.65, 0.7$, and 0.8 . The inset shows the calculated Fermi energy shift with Na doping x from the rigid-band model. (d) Experimental valence-band structure of Na_xWO_3 for $x=0.8$ obtained from HR-ARPES experiments along the highly symmetric directions. Bright areas correspond to the experimental bands. The theoretical band calculation of NaWO_3 is also shown by thin solid and dashed lines for comparison.

In Fig. 4(c), we show the valence-band-edge region at the $\Gamma(X)$ point of the highly metallic compositions (above $x=0.5$) studied here. To confirm whether the rigid-band model is appropriate or not in the highly metallic Na_xWO_3 , we have excluded the $x=0.3$ metallic composition since it is very close to MIT composition. A clear shift in the valence-band edge is observed as the Na content is increased. We have shifted the spectra (after normalizing the area under the curve), superimposed them, and determined the shift to be ~ 0.24 eV as x is varied from 0.58 to 0.8. The inset shows the theoretically computed energy shift calculated from a rigid-band model. The experimental shift (0.24 eV) is quite close to the theoretically computed shift, ~ 0.3 eV. Hollinger *et al.*¹² have measured angle-integrated spectra of Na_xWO_3 for $x=0-0.55$. From their results (see Fig. 3 in Ref. 12), it is evident that the edge of valence band moves downward as Na concentration increases from 0 to 0.55. To elucidate

whether the rigid-band model is appropriate or not, one should exclude all the compositions below MIT as they associate with complicated phenomena such as localization of bands or development of impurity bands or splitting of bands near E_F . They have not measured highly metallic compositions, which are expected to follow the rigid-band model. Although they have not quantitatively estimated the valence-band shift, the valence band qualitatively shows downward shift with increasing Na concentration similar to our results. Within a rigid-band model [see Fig. 1(d)], the band structure of both WO_3 and NaWO_3 should be identical, with E_F at different positions. As Na content increases in WO_3 , the conduction band fills up and E_F gradually moves upward. Hence, we conclude that rigid-band model is quite appropriate for highly metallic Na_xWO_3 , where the doped electrons from Na merely fill up the conduction band.

We have mapped out the band structure of Na_xWO_3 for $x=0.3, 0.58, 0.65, 0.7$, and 0.8 along the $\Gamma(X)$ - $X(M)$ and $\Gamma(X)$ - $M(R)$ directions. A typical band mapping of Na_xWO_3 for $x=0.8$ is shown in Fig. 4(d). The experimental band structure has been obtained similar to Na_xWO_3 for $x=0.025$ [Fig. 2(c)]. We also show the pseudopotential band structure of cubic NaWO_3 as thin solid and dashed lines for comparison. We see primarily four bands in the valence-band region. The experimental band structures are essentially similar for all the compounds in both the directions. The top of the valence band at 3.5 eV binding energy around the $\Gamma(X)$ point is not predicted in the band calculation. This flat feature may be dominated by the angle-integrated-type background reflecting the strong intensity of band at the $M(R)$ point. We find two flat nondispersive bands at 3.5 and 4.5 eV around the $\Gamma(X)$ point along the $\Gamma(X)$ - $X(M)$ direction. The intensity along the $\Gamma(X)$ - $M(R)$ direction at 4.5 eV arises due to angle-integrated-type background from the strong intensity of bands at $\Gamma(X)$ and vanishes with the decrease of disorder in Na_xWO_3 . Comparison of valence-band structures of $x=0.58$ and 0.8 shows that all the bands in valence-band regime move downward rigidly. Thus, with increasing x in Na_xWO_3 , the Na 3s electrons just fill the W 5d $_{t_g}$ conduction band and change the E_F position, consistent with the rigid-band model appropriate for the highly metallic compositions (above $x=0.5$) studied here. The gross features of experimental valence band at higher binding energy (4–8 eV) can be explained by the *ab initio* band-structure calculations. A small discrepancy arising between the theoretically computed band structure and experimentally derived bands can be explained by the intrinsic k_{\perp} broadening and final-state effects as discussed before. As explained before, the valence band (3–9 eV) consists of mostly O 2p character of Na_xWO_3 with a small admixture of bonding W 5d $_{e_g}$ character.

B. Near- E_F region

1. Insulating regime

To investigate the conduction band in more detail, we measured HR-ARPES spectra in the near- E_F region of Na_xWO_3 for $x=0.025$ at 130 K along both the highly symmetric directions, and the results are shown in Figs. 5(a) and

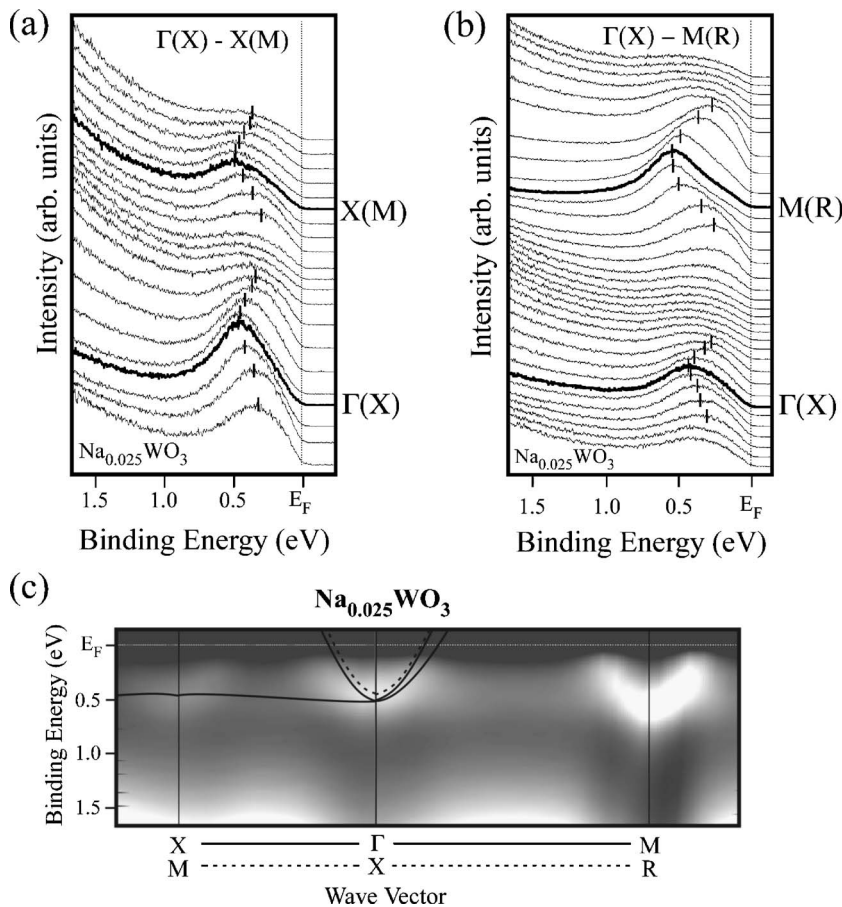


FIG. 5. HR-ARPES spectra near E_F of Na_xWO_3 for $x=0.025$ measured at 130 K along (a) $\Gamma(X)$ - $X(M)$ and (b) $\Gamma(X)$ - $M(R)$ directions. Vertical bars are a guide to eyes for band dispersion. (c) Experimental near- E_F band structure along the highly symmetric directions. Theoretical band structure of WO_3 after shifting E_F is also shown by thin solid and dashes lines for comparison.

5(b). We observe a peak near 0.45 eV at $\Gamma(X)$, which disperses upward around the $\Gamma(X)$ point. Similar feature is also observed at both $X(M)$ and $M(R)$ points. This dispersive peak represents the conduction band of Na_xWO_3 for $x=0.025$, which never crosses E_F , showing that the system is insulating. Figure 5(c) shows the plot of HR-ARPES intensity at near- E_F region. We find an electronlike pocket at the $\Gamma(X)$ point, whose dispersion agrees satisfactorily with the band calculation. The conduction band is assigned as the $W 5d_{t_2g}$ orbital from the band calculation. Similar electronlike pocket is also observed at $X(M)$ and $M(R)$ points, contrary to the band calculation. This may be due to the surface reconstruction, which we discuss later. The insulating behavior arises from the Anderson localization of all the states near E_F due to the strong disorder caused by inserting Na in WO_3 lattice. This gap arises due to the long-range interaction of the electrons trapped due to the strong disorder caused by Na doping. This would be responsible for its insulating properties. The possibility of splitting of the band due to electron correlation at the chemical potential (E_F) into two bands, originally proposed by Mott,³⁵ is unlikely in the case of Na_xWO_3 . Such correlation-driven gaps at the E_F can form only if the band has integral occupancy. This is obviously not the case for any arbitrary value of x in general; specifically, the occupancy of $W 5d$ is only a fractional 0.025 per site in Na_xWO_3 for $x=0.025$. Moreover, the Coulomb repulsion (U) is expected to be weak and the $W 5d$ bandwidth (W) is large in Na_xWO_3 to satisfy the Mott-Hubbard criterion of U/W

$\gg 1$. On the other hand, the low DOS at band bottom for the small x value favors localization of states due to disorder effects. The weak localization,³⁶ which arises from the multiple elastic scattering of carriers leading to the quantum interference, can also make the system insulating but is not feasible in the low-doped sodium tungsten bronzes. We explain this as follows. (i) If some collisions of the conduction electrons are inelastic, then the quantum interference cannot take place. These inelastic collisions can be either with other conduction electrons or with phonons above the Debye temperature. Hence, with variation of temperature, one should see an insulator-to-metal-like change, which does not occur in sodium tungsten bronzes. (ii) This effect is significant when the mean free path l is small and thus typically seen in noncrystalline materials. There are few papers on the development of surface superconductivity in low-doped sodium tungsten bronzes. It was believed that Na_xWO_3 with a very low Na concentration is a possible system in which the structure is modulated in such a way so that superconductivity occurs at the surface only without propagating into bulk. Reich and Tsabba³⁷ reported surface superconductivity with T_c as high as 91 K in the lightly doped sodium tungsten bronzes, $\text{Na}_{0.05}\text{WO}_3$. Even if we do not find surface superconductivity in $\text{Na}_{0.025}\text{WO}_3$, we expect that at least the surface should be metallic as this composition is close to superconducting composition of $x=0.05$. However, we did not find any finite DOS at E_F measured at 130 K in this system employing HR-ARPES measurements in both He I and He II photons. Hence, we conclude that there is no such supercon-

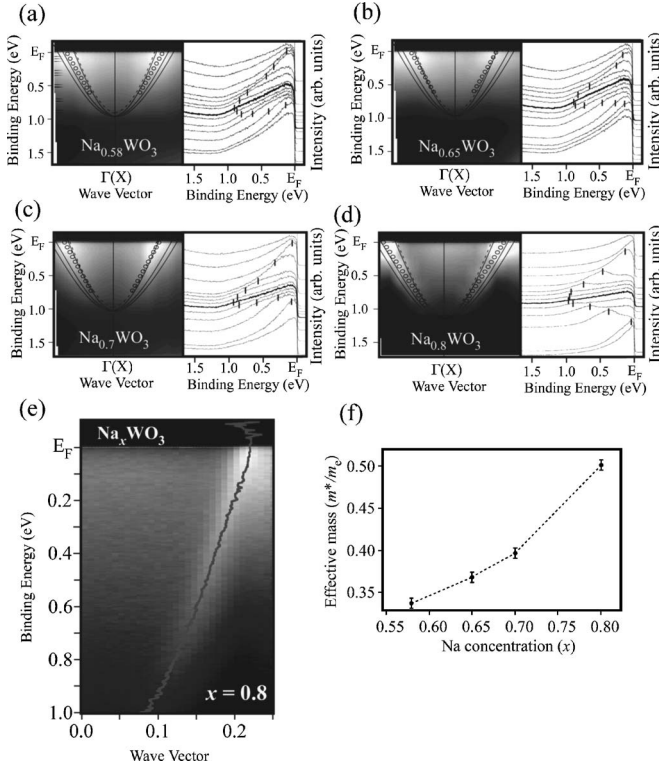


FIG. 6. Experimental near- E_F HR-ARPES spectra along with the experimental band structure of Na_xWO_3 for (a) $x=0.58$, (b) $x=0.65$, (c) $x=0.7$, and (d) $x=0.8$ measured at 14 K. Only the $\Gamma(X)$ region is shown from the $\Gamma(X)$ - $M(R)$ direction of BZ. Vertical bars are a guide to eyes for band dispersion in EDCs. Theoretical band structure of NaWO_3 is also shown in the intensity map by thin, solid, and dashed lines for comparison. Open circles show the highest intensity in experimental band mapping. (e) Near- E_F momentum distribution curve (MDC) of Na_xWO_3 for $x=0.8$. The gray solid line represents the MDC peak dispersion. The Fermi velocity v_F is determined from the slope $(\delta E/\delta k)$ at E_F . (f) The effective mass (m^*/m_e) with respect to Na concentration in Na_xWO_3 .

ductivity on the surface of the lightly doped sodium tungsten bronzes.

2. Metallic regime

We have carried out HR-ARPES measurements with a smaller energy interval and a higher signal-to-noise ratio to study the electronic structure near E_F . Figures 6(a)–6(d) show the near- E_F HR-ARPES spectra along with the intensity as a function of the wave vector and the binding energy of Na_xWO_3 for $x=0.58$, 0.65, 0.7, and 0.8 measured at 14 K with He 1α photons. From the energy distributive curves (EDCs), we observe a very weak broad feature near 0.9–1.0 eV at $\Gamma(X)$, which disperse upward to form an electronlike pocket at $\Gamma(X)$ for all compositions of x . There is no signature of such a feature at $X(M)$, or $M(R)$, as observed in its insulating counterpart. We have shown only the $\Gamma(X)$ region in figures due to the presence of band dispersion near E_F at $\Gamma(X)$. As the Na concentration increases, this feature becomes very prominent, as shown in EDC of Fig. 6(d). This behavior may be due to the decrease of disorder with increas-

ing x in the system. From the figures, we find that the bottom of conduction band lies roughly around 0.9–1.0 eV below E_F . The exact position of the band bottom is difficult to determine due to the very low spectral intensity at its bottom. Nevertheless, it is clear that the conduction-band bottom moves downward with Na concentration similar to the trend seen for the valence band [Fig. 4(c)]. This can be explained by considering the simple rigid-band shift. Since the determination of the exact position of band bottom has much more ambiguity, it is difficult to determine quantitatively the shift of the band bottom from $x=0.58$ to 0.8. Previous reports^{14,38–40} along with Hollinger *et al.*¹² demonstrated that the bandwidth of occupied conduction states appears to be almost independent of Na concentration, which is not supported by our results. Since the DOS at band bottom is very low and the background is high, hence it was impossible to get the exact bandwidth of occupied states from previous angle-integrated measurements. Our results of band dispersion in insulating phase [see Fig. 5(c)] and metallic phase [see Figs. 6(a)–6(d)] clearly show that the bandwidth of occupied states increases gradually as Na concentration increases. This behavior can be well understood by the rigid-band model. The HR-ARPES intensity map shows an electronlike pocket at $\Gamma(X)$, whose linear dispersion at E_F agrees satisfactorily with the band calculation. We find a clear variation in the spectral intensity at E_F , which suggests that the band crosses E_F at the highest intensity (k_F) region. No signature of impurity band (level) near E_F is seen in Figs. 6(a)–6(d), which rules out the development of a Na-induced impurity band (level). Hollinger *et al.*¹² concluded that the MIT associated in Na_xWO_3 is mainly due to the Anderson localization (disorder driven) and claimed that the evolution of impurity band seems to be filled up for very low Na concentration. Our results for very low concentration of Na ($x=0.025$) show a well-defined band dispersion which agrees well with the $W 5d_{2g}$ band calculation. We do not observe any extra levels or bands in our experiments to support their claim. In fact, due to the localization of states, other phenomena such as polaron formation and Anderson localization at E_F occur in this sodium tungsten bronze, which we have already discussed. Hence, we conclude that the previous speculation regarding MIT being due to the development of Na-induced impurity band (level) is not supported by our results.

In the rigid-band model with a spherical Fermi surface and rigid parabolic DOS, the density of states $N(E)$ is proportional to $E^{1/2}$. It is assumed that all sodium atoms are ionized in Na_xWO_3 ; hence, $N(E_F)$, the density of states at E_F , is proportional to $x^{1/3}$. However, the physical properties including the magnetic susceptibility and the specific-heat coefficient⁴¹ γ were found to vary linearly with x . We extrapolated the band dispersion from the highest intensity points of the band mapping [shown as open circles in Figs. 6(a)–6(d)] and find that the conduction bandwidth expands with increasing x ; the experimental band dispersion is not free electron-like parabolic as proposed before. The *ab initio* band-structure results also show linear band dispersion as observed experimentally. The expansion of conduction band can be well explained by the linear increase in the density of

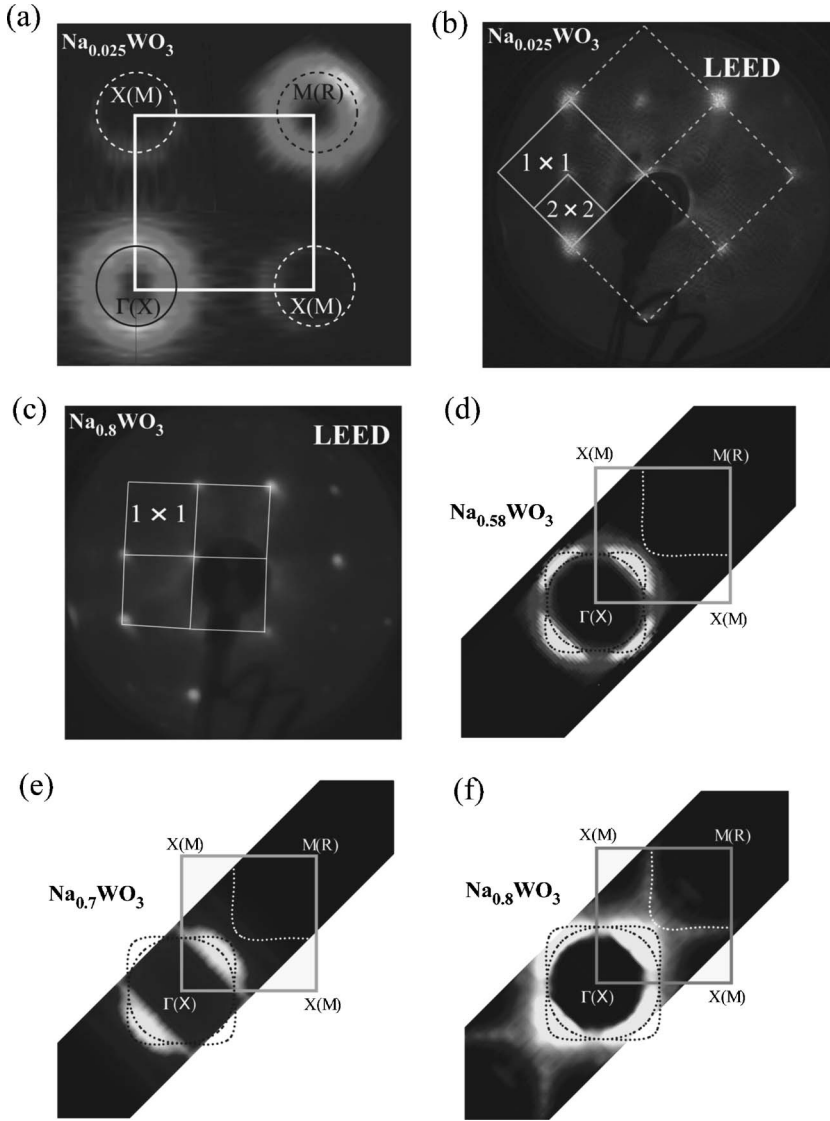


FIG. 7. (a) Remnant Fermi surfaces of Na_xWO_3 for $x=0.025$ at 130 K in the first BZ. Solid and dashed circles show the highest intensity points. (b) LEED pattern of (001) cleaved surface of Na_xWO_3 for $x=0.025$ measured with primary energy of 54 eV at 130 K. It shows the 1×1 bulk and the 2×2 surface superlattice spots. (c) LEED pattern of (001) cleaved surface of Na_xWO_3 for $x=0.8$ measured with primary energy of 106 eV at 14 K. Fermi surfaces of Na_xWO_3 for (d) $x=0.58$, (e) $x=0.7$, and (f) $x=0.8$ showing electronlike pocket at the $\Gamma(X)$ point. Dotted lines around the $\Gamma(X)$ point are the calculated Fermi surface(s) (on $\Gamma X M X$ and $X M R M$ planes) for fractional Na concentration based on the rigid-band model.

states of the conduction band with increasing x in Na_xWO_3 . This explanation fits well with the x -dependent behavior of the specific heat and the magnetic susceptibility, which vary linearly with x for highly metallic Na_xWO_3 . The heat-capacity data⁴¹ show that the effective mass (m^*) of conduction electrons increases monotonically with x . We determined the effective mass from the Fermi velocity v_F at E_F , as shown in Fig. 6(e), for $x=0.8$ and found a similar monotonic increase in the effective mass [Fig. 6(f)] of the conduction electrons for all x . The band mass is less than the free-electron mass m_0 and agrees quantitatively with the mass found from other experiments.⁴²

C. Fermi-surface topology

1. Insulating regime

In Fig. 7(a), we show the HR-ARPES-intensity plot at E_F as a function of two-dimensional (2D) wave vector. The intensity is obtained by integrating the spectral weight within 80 meV with respect to E_F and symmetrized on assuming the cubic symmetry. The conduction band arising from the

$W 5d_{t_2g}$ orbital disperses upward (Fig. 5) but never crosses E_F . Recently, a new concept⁴³ has been introduced for the analysis of photoemission spectra—the remnant Fermi surface, which can be measured even in insulating systems, where conventional FS does not exist. Remnant FS is the locus of points in k space, where the photoemission intensity associated with the near- E_F peak reduced drastically due to the presence of disorder or electron correlations. For an ordinary metal, these points would correspond to the conventional FS. Our finding reveals a remnant FS in Na_xWO_3 for $x=0.025$ even though it shows insulating behavior and arises due to the gap opening at the E_F . Similar remnant FS is observed in other insulator, $\text{Ca}_2\text{CuO}_2\text{Cl}_2$.⁴³ From the high-quality data near E_F , we establish that the remnant FS observed at the $\Gamma(X)$ point in the insulating phase has a shape similar to the real FS in metallic sodium tungsten bronzes which one expect in the absence of any disorder in metallic phase and matches well to the band calculation. We find similar remnant FS at $X(M)$ and $M(R)$ and we infer that this is due to the surface reconstruction. We carried out the low-energy electron diffraction (LEED) for the (001) cleaved surface with primary energy of 54 eV at 130 K and the result is

shown in Fig. 7(b). In the LEED pattern, we see the 1×1 bulk and the 2×2 surface superlattice spots. The 2×2 superlattice spots regenerate the $X(M)$ and $M(R)$ points as a new $\Gamma(X)$ point in HR-ARPES. Hence the surface reconstruction is confirmed from our LEED measurement. Now we discuss in more detail the surface reconstruction, which may create 2D electronic states on the first few layers different from the bulk states. Such surface-reconstruction-derived bands were found in the HR-ARPES spectra of Sr_2RuO_4 .⁴⁴ The rotation and deformation of the WO_6 octahedra in Na_xWO_3 for $x=0.025$ give rise to the orthorhombic crystal structure. In the bulk, the rotation is small and we think that the rotation of the WO_6 octahedra increases at surface due to the reduced atomic coordination, which is responsible for the surface reconstruction in Na_xWO_3 for $x=0.025$ as similarly observed in Sr_2RuO_4 .⁴⁴

2. Metallic regime

In Fig. 7(c), we show the LEED measurement of metallic Na_xWO_3 for $x=0.8$ with primary energy of 106 eV at 14 K. The LEED pattern shows only 1×1 bulk spots without any signature of superlattice spots. This removes the possibility of surface reconstruction in metallic system as compared to its insulating counterpart. The HR-ARPES-intensity plots at E_F for Na_xWO_3 ($x=0.58, 0.7, \text{ and } 0.8$) as a function of the 2D wave vector are shown in Figs. 7(d)–7(f). The intensity is obtained by integrating the spectral weight within 20 meV with respect to E_F . We calculated the Fermi surface(s) (on ΓXMX and $XMRM$ planes) for fractional Na concentration in Na_xWO_3 ($x=0.58, 0.7, \text{ and } 0.8$) assuming the rigid-band shifts, which are shown by dotted lines. We observe one spherical electronlike Fermi surface centered at the $\Gamma(X)$ point, which is covered with another squarelike Fermi surface. Along the $\Gamma(X)$ - $X(M)$ direction, we find only one k_F point, while along the $\Gamma(X)$ - $M(R)$ direction there are two distinct k_F points. These two Fermi surfaces are attributed to the $W 5d_{2g}$ photons. From the energy distributive bands. On increasing the Na concentration, the $\text{Na } 3s$ electrons are transferred to the $W 5d_{2g}$ band at E_F . Hence, the volume of the Fermi surface gradually increases in accordance with the increase of the Na concentration. The squarelike Fermi surface centered at the M point is not visible in Na_xWO_3 for $x=0.58$ and 0.7 but is prominent in $x=0.8$. This Fermi surface arises from one single band, whereas the Fermi sur-

face(s) observed at $\Gamma(X)$ point are from three bands (two from ΓXMX and one from the $XMRM$ planes) and hence the intensity is much more enhanced around the $\Gamma(X)$ point in the HR-ARPES experiment. The volume of calculated Fermi surface and experimental Fermi surface matches well for all highly metallic compositions studied here. A rigid shift of the Fermi energy is found to give a qualitatively good description of the FS.

V. CONCLUSION

We have carried out high-resolution angle-resolved photoemission spectroscopy on Na_xWO_3 for $x=0.025, 0.3, 0.58, 0.65, 0.7, \text{ and } 0.8$. The experimentally determined valence-band structure has been compared with the results of *ab initio* band-structure calculation. It is found that in insulating Na_xWO_3 , the near- E_F states are localized (Anderson localization) due to the strong disorder caused by the random distribution of Na^+ ions in the WO_3 lattice. While the presence of an impurity band (level) induced by Na doping is often invoked to explain the insulating state found at low concentrations, there is no signature of impurity band (level) found in our results to support this idea. Due to this disorder and Anderson localization effect, there is a long-range Coulomb interaction of conduction electrons; as a result, the system is insulating. We found a direct evidence of polaron formation from the temperature dependence of the photoemission spectra. In the metallic regime, we found that the rigid shift of band structure can well explain the metallic Na_xWO_3 band structure with respect to Na doping. The linear dispersion of the conduction band at E_F explains the linear variation of thermodynamic properties including the specific heat and magnetic susceptibility. We observed electronlike Fermi surface at the $\Gamma(X)$ point as predicted from band calculation, and the Fermi surface gradually increases with increasing Na concentration due to $W 5d_{2g}$ band filling in highly metallic systems. A rigid shift of the Fermi energy is found to give a qualitatively good description of the Fermi surface.

ACKNOWLEDGMENTS

This work is supported by grants from the JSPS, the MEXT, and the CREST of Japan. S.R. thanks the JSPS for the financial support. The work at Rutgers was supported by NSF-DMR grants.

*Electronic address: raj@arpes.phys.tohoku.ac.jp

[†]Also at Jawaharlal Nehru Centre for Advanced Scientific Research, Bangalore 560 054, India.

¹C. G. Granqvist, *Handbook of Inorganic Electrochromic Materials* (Elsevier, Amsterdam, 1995).

²P. M. S. Monk, R. J. Mortimer, and D. R. Rosseinsky, *Electrochromism: Fundamentals and Applications* (VCH, Weinheim, 1995).

³J. B. Goodenough, in *Progress in Solid State Chemistry*, edited by

H. Reiss (Pergamon, Oxford, 1971), Vol. 5, pp. 145–399.

⁴H. R. Shanks, P. H. Slides, and G. C. Danielson, *Adv. Chem. Ser.* **39**, 237 (1963).

⁵A. S. Ribnick, B. Post, and E. Banks, *Adv. Chem. Ser.* **39**, 246 (1963).

⁶B. W. Brown and E. Banks, *J. Am. Chem. Soc.* **76**, 963 (1954).

⁷P. W. Anderson, *Phys. Rev.* **109**, 1492 (1958).

⁸D. P. Tunstall and W. Ramage, *J. Phys. C* **13**, 725 (1980).

⁹N. F. Mott, *Metal-Insulator Transitions* (Taylor & Francis, Lon-

- don, 1990).
- ¹⁰R. L. Benbow and Z. Hurych, *Phys. Rev. B* **17**, 4527 (1978).
- ¹¹M. D. Hill and R. G. Egdell, *J. Phys. C* **16**, 6205 (1983).
- ¹²G. Hollinger, P. Pertosa, J. P. Doumerc, F. J. Himpsel, and B. Reihl, *Phys. Rev. B* **32**, 1987 (1985).
- ¹³T. Wolfram and L. Sutcu, *Phys. Rev. B* **31**, 7680 (1985).
- ¹⁴H. Höchst, R. D. Bringans, and H. R. Shanks, *Phys. Rev. B* **26**, 1702 (1982).
- ¹⁵L. Koop, B. N. Harmon, and S. H. Liu, *Solid State Commun.* **22**, 677 (1977).
- ¹⁶N. E. Christensen and A. R. Mackintosh, *Phys. Rev. B* **35**, 8246 (1987).
- ¹⁷M. G. Stachiotti, F. Corà, C. R. A. Catlow, and C. O. Rodriguez, *Phys. Rev. B* **55**, 7508 (1997).
- ¹⁸S. Oishi, N. Endo, and K. Kiajima, *Nippon Kagaku Kaishi* **11**, 891 (1995).
- ¹⁹H. R. Shanks, *J. Cryst. Growth* **13/14**, 433 (1972).
- ²⁰P. E. Blöchl, *Phys. Rev. B* **50**, 17953 (1994).
- ²¹G. Kresse and D. Joubert, *Phys. Rev. B* **59**, 1758 (1999).
- ²²G. Kresse and J. Furthmüller, *Phys. Rev. B* **54**, 11169 (1996); *Comput. Mater. Sci.* **6**, 15 (1996).
- ²³V. N. Strocov, H. I. Starnberg, P. O. Nilsson, and L. J. Holleboom, *J. Phys.: Condens. Matter* **8**, 7549 (1996).
- ²⁴V. N. Strocov, H. I. Starnberg, and P. O. Nilsson, *Phys. Rev. B* **56**, 1717 (1997).
- ²⁵N. Barrett, E. E. Krasovskii, J.-M. Themlin, and V. N. Strocov, *Phys. Rev. B* **71**, 035427 (2005).
- ²⁶V. N. Strocov, *J. Electron Spectrosc. Relat. Phenom.* **130**, 65 (2003).
- ²⁷V. N. Strocov, *Int. J. Mod. Phys. B* **9**, 1755 (1995).
- ²⁸V. N. Strocov, H. I. Starnberg, and P. O. Nilsson, *J. Phys.: Condens. Matter* **8**, 7539 (1996).
- ²⁹O. F. Schirmer and E. Salje, *Solid State Commun.* **33**, 333 (1980); *J. Phys. C* **13**, L1067 (1980).
- ³⁰E. Salje and B. Guttler, *Philos. Mag. B* **50**, 607 (1984).
- ³¹R. G. Egdell and G. B. Jones, *J. Solid State Chem.* **81**, 137 (1989).
- ³²H. DeRaedt and A. Lagendijk, *Phys. Rev. B* **27**, 6097 (1983); H. Lowen, *ibid.* **37**, 8661 (1988); J. Ranninger and U. Thibblin, *ibid.* **45**, 7730 (1992).
- ³³G. F. Koster and J. C. Slater, *Phys. Rev.* **95**, 1167 (1954).
- ³⁴N. Shanthi and D. D. Sarma, *Phys. Rev. B* **57**, 2153 (1998).
- ³⁵N. F. Mott, *Philos. Mag.* **35**, 111 (1977).
- ³⁶G. Bergmann, *Phys. Rev. B* **28**, 2914 (1983); *Phys. Rep.* **107**, 1 (1984).
- ³⁷S. Reich and Y. Tsabba, *Eur. Phys. J. B* **9**, 1 (1999).
- ³⁸M. Campagna, G. K. Wertheim, H. R. Shanks, F. Zumsteg, and E. Banks, *Phys. Rev. Lett.* **34**, 738 (1975).
- ³⁹H. Höchst, R. D. Bringans, H. R. Shanks, and P. Steiner, *Solid State Commun.* **34**, 41 (1980).
- ⁴⁰G. K. Wertheim and J. N. Chazalviel, *Solid State Commun.* **40**, 931 (1981).
- ⁴¹F. C. Zumsteg, *Phys. Rev. B* **14**, 1406 (1976).
- ⁴²M. Kielwein, K. Saiki, G. Roth, J. Fink, G. Paasch, and R. G. Egdell, *Phys. Rev. B* **51**, 10320 (1995).
- ⁴³F. Ronning, C. Kim, D. L. Feng, D. S. Marshall, A. G. Loeser, L. L. Miller, J. N. Eckstein, I. Bozovic, and Z. X. Shen, *Science* **282**, 2067 (1998).
- ⁴⁴R. Matzdorf, Z. Fang, Ismail, J. Zhang, T. Kimara, Y. Tokura, K. Terakura, and E. W. Plummer, *Science* **289**, 746 (2000).